Sound & Vibration 2026, 60(3), 4017.
doi: https://doi.org/10.59400/sv4017

Article

Optimization and experimental study of low-frequency sound absorption performance for modified sonic black hole

Ziyan Chen, Qibo Mao*, Lihua Peng

School of Power and Energy, Nanchang Hangkong University, Nanchang 330063, China

*** Corresponding author:** Qibo Mao, qbmao@nchu.edu.cn

CITATION

Chen Z, Mao Q, Peng L. Optimization and experimental study of low-frequency sound absorption performance for modified sonic black hole. Sound & Vibration. 2026; 60(3): 4017. https://doi.org/10.59400/sv4017

ARTICLE INFO

Received: 9 February 2026
Revised: 20 March 2026
Accepted: 24 March 2026
Available online: 6 May 2026

Abstract: The design of a sound absorber with simultaneous broadband and low-frequency absorption is still difficult to achieve. Most existing noise reduction techniques target only a single aspect of the acoustic performance. The difficulty lies in the inherent trade-off between compact size, broad bandwidth, and effective low-frequency absorption. To overcome these issues, this study proposes a modified sonic black hole (SBH) to enhance the conventional SBH structure's low-frequency broadband sound absorption capabilities. By introducing the concept of equivalent length, this study adjusts only the opening area of the SBH structure without increasing its length, thereby equating the modified SBH to an original SBH with a longer geometric length. This equivalent extension enhances the coupling between the structure and low-frequency sound waves, thereby improving the low-frequency sound absorption performance. Theoretical modeling and simulation analysis demonstrate that reducing the SBH inlet diameter (or ring maximum inner diameter) can effectively improve the SBH low-frequency sound absorption effect. Furthermore, experimental comparisons of modified SBHs under different inlet diameters reveal that reducing the diameter from a fully open (95 mm) to 30 mm reduces the SBH's first natural frequency from 615 Hz to 225 Hz, demonstrating a marked improvement in low-frequency sound absorption performance. The proposed modified SBH concept provides a promising solution for low frequency and broadband noise control.

Keywords: modified sonic black hole; low-frequency; sound absorption; opening diameter; resonance frequency shift

1. Introduction

As a common source of noise in daily life, low-frequency noise, because of its long wavelength, is more difficult to interact with structures and is absorbed effectively. Furthermore, the dissipation of low-frequency noise in the air is much weaker than that of high-frequency noise, and conventional sound-absorbing materials also have poor sound absorption efficiency for it. Therefore, how to effectively reduce low-frequency noise has been a key breakthrough in noise control for a long time. Generally speaking, there are three main types of traditional sound-absorbing methods. One type is the traditional porous materials. They mainly convert sound energy into thermal energy through the viscous effect [1]. Common materials include polyester fiber, polyurethane foam and mineral wool. However, the thickness significantly restricts their ability to absorb low-frequency sound—effective low-frequency absorption requires an impractically large material thickness. Resonant sound-absorbing structures

rely on the resonance principle to generate vibration and friction loss near the resonance frequency, thereby absorbing sound efficiently. These include membrane resonant structures and Helmholtz resonant structures, among which microperforated panels (MPPs) are widely used in practical buildings. Although these types of structures can address noise at specific frequencies, their sound absorption bandwidth is relatively narrow. Acoustic metamaterial sound-absorbing structures manipulate sound waves through artificially designed special structural units, achieving sound-absorbing effects that natural materials cannot match [2,3].

Recently, the sonic black hole (SBH) effect for sound reduction, which was first proposed by Mironov and Pislyakov [4], has gained more and more attention. The characteristics of the SBH are the placement of annular baffles of varying sizes inside the duct according to a specific pattern, which enables a gradient change in duct admittance and thereby achieves the attenuation of sound waves inside the duct. This design adjusts the inner radii of the thin plates such that the cross-section inside the duct exhibits a linear or quadratic power-law variation. As a result, the speed at which sound waves transit through the duct progressively reduces to zero; sound waves cannot be reflected because they cannot transit to the end of the duct within a finite time, thus achieving the goal of absorbing sound waves without the need for additional sound-absorbing materials. Although SBH can achieve broadband, high-efficiency sound absorption at thicknesses far smaller than the wavelength, they also suffer from poor low-frequency absorption performance due to limitations in the number of units and manufacturing precision. The traditional sound absorption methods mentioned previously, including sound-absorbing materials and resonant sound-absorbing structures, can also optimize sound absorption performance through structural design. However, as the number of component resonators increases, their configurations tend to become more complex.

Research on SBHs reveals that there are two primary methods to effectively enhance their sound absorption performance. Optimizing the SBH's geometric structure is one strategy. For instance, Su et al. [5] discovered that while adding more internal embedded loops within the SBH enhances mid-to-high frequencies sound absorption performance but increases low-frequency reflections. Optimizing the structural design to increase flow velocity gradients and pressure differentials at low frequencies improves the SBH's ability to suppress low-frequency sound waves. Peng et al. [6] combined multiple SBHs of varying lengths through spatial partitioning, leveraging their distinct resonance frequencies to lower the cut-off frequency and enhance the sound absorption coefficient. Bednarik and Cervenka [7] conducted research on the theoretical model and analytical solution of SBH with a rectangular cross-section, providing an accurate theoretical tool for optimizing the geometric structure design of SBH. Yu et al. [8] proposed a truncated rectangular SBH structure. Using the effective medium theory and experiments, they respectively studied the effects of various truncation radii on the sound absorption capabilities of traditional SBH structures, truncated SBH structures, and those filled with porous materials. Deng et al. [9] proposed a plug-in SBH. As an independently manufactured axisymmetric insert, it requires no modification to the duct geometry, accommodates ducts of any

material or shape, and shows a lower reflection coefficient across a wide range of frequencies. Li et al. [10] demonstrated that coupling hexagonal SBH units with different power-law exponents through resonance coupling effects can significantly broaden the low-frequency absorption bandwidth. Another approach is combining SBH with other sound-absorbing materials or structures to achieve enhanced sound absorption performance. Zhang et al. [11] integrated a synergistic composite sonic black hole structure (CSBH) by combining the SBH, gradient MPPs, and porous materials. Results indicate that this structure attains almost the best sound absorption beginning at 307 Hz. Peng and Mao [12] combined the Helmholtz Resonator (HR) and the SBH neck. Through theoretical and experimental analysis, they were able to effectively absorb sound in a wide frequency range that did not include HR resonance frequencies. Liang et al. [13, 14] suggested a better SBH structure that embeds a microperforated plate into a labyrinth unit with multiple resonant cavities. The sound absorption effect of this structure can be evaluated by analyzing the allocation of sound pressure and velocity. Jin et al. [15] proposed a labyrinth-like structure that combined the ideas of Herschel-Quincke (HQ) tubes and acoustic black holes (ABH), enabling efficient noise reduction while maintaining ventilation. Meng et al. [16] proposed a composite sound-absorbing structure combining ABHs with MPPs. By partitioning the structure into multiple Helmholtz resonators using MPPs, and integrating the sound-focusing effect of ABHs with the impedance-modulating function of MPPs, they achieved broadband sound absorption. Chen et al. [17] combined a labyrinth metasurface with the end of a rectangular SBH embedded in porous material, utilizing metasurface resonance to further enhance the low-frequency sound absorption mechanism. Petrover and Baz [18, 19] employed a functionally graded perforated ring (FGPR) within the ABH, utilizing the flow through the perforations to generate intrinsic energy dissipation, thereby accelerating the wave velocity to zero. Simultaneously, an acoustic absorption layer can be inserted between the rings to further enhance broadband sound absorption capabilities. Li et al. [20] studied the effect of perforated acoustic boundaries on SBH, proposed an SBH-pb structure, and analyzed the perforated boundary (PB) with a rear cavity by using the transfer matrix method (TMM). Ou and Zhao [21] optimized the SBH by integrating it with a basic sound-absorbing unit comprising microperforated plates, folded cavities, and slits, achieving broadband sound absorption through the generation of additional resonance peaks. Wu et al. [22] employed a membrane-type acoustic metamaterial as the back cavity of the SBH, significantly enhancing its low-frequency sound absorption performance through the coupling of energy-harvesting mechanisms with localized resonance effects.

Additionally, scholars have also investigated the performance of SBH in other applications. Zhang et al. [23] investigated the muffling characteristics and mechanisms of SBHs. When connected as a side branch to the main duct, a linear SBH exhibited multi-peak, broadband muffling properties. Maury et al. [24] compared Opened SBH (O-SBH), Closed SBH (C-SBH), and MPP-SBH, demonstrating that O-SBH (particularly MPP-SBH) can function simultaneously as both a muffler and an acoustic sensor, amplifying weak signals while controlling noise. Zhou et al. [25] proposed a

methodology for improving contactless sensing by using the SBH metamaterial structure, enabling weak signal amplification and fault diagnosis in rotating machinery. Peng et al. [26] and Mao and Peng [27] verified the capability of the SBH for an acoustic energy harvester (AEH). When the SBH is combined with an electrodynamic loudspeaker or a circular piezoelectric composite sheet, this AEH can convert captured acoustic energy into electrical energy.

Different from previous studies, we plan to improve SBH's low-frequency sound absorption capabilities without increasing its complexity (e.g., by adding other sound-absorbing structures such as HR or MMP). This paper proposed a modified SBH by reducing its open area to reduce the effective sound absorption frequency band without increasing the geometric length of the SBH. Umnova et al. [28] indicate that the front ring plate's resonance frequency establishes the high-frequency sound absorption range. As the inner diameter of the entrance ring increases, the sound absorption performance for high frequencies becomes more significant. The modified SBH structure proposed in this paper is equivalent to the latter half obtained by truncating the original SBH at a certain middle position. Thus, for the same length, the smaller the cross-sectional area of the open end, the better the improvement in low-frequency sound absorption performance. In contrast, the omission of the front annular plates inevitably results in the loss of part of the high-frequency sound absorption capacity. The paper is structured as follows: in Section 2, the acoustic impedance model for the modified SBH is established by using the TMM, and derived an expression for the sound absorption coefficient; in Section 3, theoretical analysis and numerical simulation are used to examine the proposed modified SBH's sound absorption performance and mechanism; in Section 4, experiments are performed to verify the proposed modified SBH, and it confirmed that when the diameter decreased from the fully open state to 30 mm, the first frequency of the structure dropped from 615 Hz to 225 Hz. Its low-frequency sound absorption performance significantly improved; the primary conclusions of this paper are finally presented in Section 5.

2. Theoretical model of SBH

A series of rigid rings with a specific internal radius variation pattern is arranged at fixed intervals within a cylindrical cavity to form an SBH absorber. To improve the conventional SBH structures' ability to absorb low-frequency sound, this study proposes new SBHs with different inlet opening radius, hence termed a modified SBH. **Figure 1a** presents the three-dimensional schematic illustration of the modified SBH.

In the theoretical model, the thickness of the rigid rings is assumed to be sufficiently small, such that its influence on the overall acoustic performance can be neglected. **Figure 1b** illustrates the two-dimensional cross-section of the proposed modified SBH absorber. Assume that the internal radius of the rings varies linearly. The internal radius r_n of the nth ring satisfies the following relation:

$$r_n = \frac{R_{inlet} - r_{\text{end}}}{L_{SBH}} \left(L_{SBH} - \sum\nolimits_{i=1}^{n-1} d_i \right) + r_{end},\ n = 1, 2, \ldots, N \tag{1}$$

where r_n is the n_{th} ring's internal radius; r_{end} is the radius of the closed end; R_{inlet}

and L_{SBH} denote the SBH structure's opening radius and axial length; d_i represents the spacing between the i_{th} and $(i+1)_{\text{th}}$ rings.

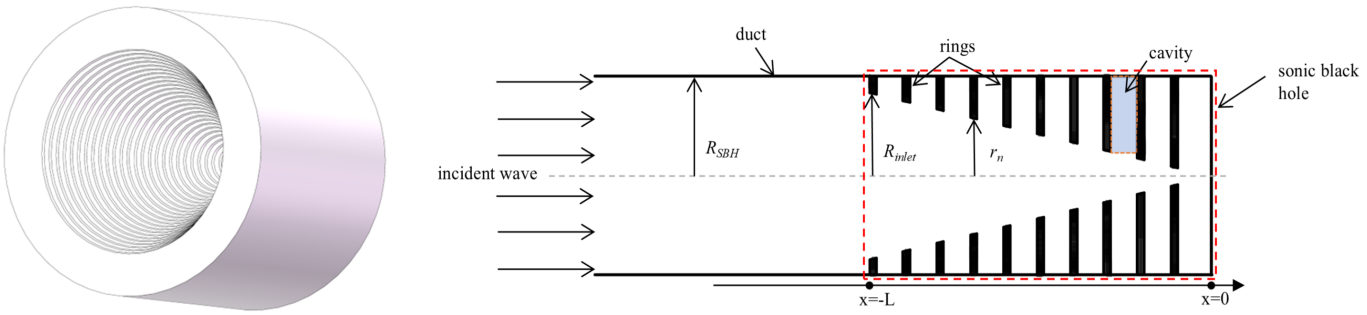

(a) **(b)**

Figure 1. **(a)** Three-dimensional schematic illustration of modified SBH; **(b)** Two-dimensional cross-sectional schematic of SBH absorber structure.

Assuming that sound waves propagate through the SBH as plane waves, and the SBH's characteristic dimensions are significantly smaller than the acoustic wavelength at the frequencies of interest. The TMM can be used to precisely characterize the sound absorption performance of the structure by determining the acoustic impedance of the SBH.

Based on the number of rings, the SBH structure can be discretized into N serially-connected cylindrical duct segments, as illustrated in **Figure 1b**. Each segment consists of two parts: the annular cavity formed between adjacent rings and the central truncated cone. Throughout this paper, we adopt the time convention $e^{j\omega t}$ for the wave field. The transfer matrix of the n_{th} segment can be expressed as follows [29]:

$$\begin{bmatrix} p_{n-1} \\ u_{n-1} \end{bmatrix} = \begin{bmatrix} cos\,(kd_n) & j\frac{Z_0}{S_n} sin\,(kd_n) \\ j\frac{S_n}{Z_0} sin\,(kd_n) & cos\,(kd_n) \end{bmatrix} \begin{bmatrix} 1 & 0 \\ Y_n & 1 \end{bmatrix} \begin{bmatrix} p_n \\ u_n \end{bmatrix}, \; n = 1, 2, \ldots, N \quad (2)$$

where p_{n-1}, u_{n-1} and p_n, u_n are the acoustic pressure and particle velocity at the $(n-1)_{\text{th}}$ and n_{th} rings, respectively; d_n is the spacing between the $(n-1)_{\text{th}}$ and n_{th} rings; $S_n = \pi r_n^2$ is the radial cross-sectional area of the n_{th} ring; $Z_0 = \rho_0 c_0$ is the characteristic impedance of air, where ρ_0 is the air density, typically valued at 1.21 kg/m^3, and c_0 is the speed of sound, valued at 340 m/s; $k = \frac{\omega}{c}$ is the complex wavenumber, ω is the angular frequency and $c = c_0(1 + j\zeta)$ is the complex sound speed accounting for damping, j is the imaginary unit, ζ is the damping loss factor introduced to account for the thermoviscous and structural damping effects in the SBH. According to previous studies [4,7,29–31], the effect of damping on SBH performance has been investigated. In most studies, the damping values were assumed based on empirical data, and Y_n is the cavity admittance between the n_{th} and $(n-1)_{\text{th}}$ rings.

According to Guasch et al. [29], Y_n can be expressed as:

$$Y_n = j\frac{k}{Z_0} V_n^{cav} \quad (3)$$

where V_n^{cav} is the n_{th} cavity's volume. V_n^{cav} is calculated as the difference between the

volumes of the n_{th} cylinder and the truncated cone,

$$V_n^{cav} = \pi d_n \left[R^2 - \frac{1}{3}\left(r_n^2 + r_n r_{n+1} + r_{n+1}^2 \right) \right]. \tag{4}$$

From the preceding analysis, it follows that the global transfer matrix of the SBH structure can be derived through the concatenation of individual cylindrical segment matrices using the TMM, yielding:

$$\begin{bmatrix} p_0 \\ u_0 \end{bmatrix} = \prod_{n=1}^{N} T_n \begin{bmatrix} p_N \\ u_N \end{bmatrix} = T_{SBH} \begin{bmatrix} p_N \\ u_N \end{bmatrix}, \tag{5}$$

where p_0, u_0 and p_N, u_N represent the sound pressure and particle velocity at the inlet and rigid termination, respectively. $T_n = \begin{bmatrix} cos\,(kd_n) & j\,sin\,(kd_n)\,Z_0/S_n \\ j\,sin\,(kd_n)\,S_n/Z_0 & cos\,(kd_n) \end{bmatrix} \begin{bmatrix} 1 & 0 \\ Y_n & 1 \end{bmatrix}$, $T_{SBH} = \prod_{n=1}^{N} T_n$ is the global transfer matrix of the SBH.

In practical implementations where the SBH structure terminates at a rigid wall boundary, the acoustic particle velocity at the termination can be set to zero (u_N = 0). Substituting this condition into Equation (5) yields the effective acoustic input impedance Z_{in} of the SBH structure as:

$$Z_{in} = \frac{p_0}{u_0} = \frac{T_{SBH}(1,1)}{T_{SBH}(2,1)} \tag{6}$$

where T_{SBH}(1,1) and T_{SBH}(2,1) are elements of T_{SBH}.

From Equation (6), the effective input impedance Z_{in} can be derived. Then the SBH's sound absorption coefficient α can be derived as:

$$\alpha = 1 - \left| \frac{Z_{in} - \frac{Z_0}{S_0}}{Z_{in} + \frac{Z_0}{S_0}} \right|^2 \tag{7}$$

3. Sound absorption performance and mechanism analysis

3.1. Comparison of sound absorption performance

To verify that the suggested modified SBH performs better at absorbing low-frequency sound, throughout this research, we set the number of built-in rigid rings as N = 30, and the SBH structure's length as L_{SBH} = 90 mm. In contrast to the original SBH with a fully open diameter of D = 95 mm, we analyzed the modified SBH's sound absorption capabilities with inlet opening diameters of D = 30 mm, 50 mm, 70 mm, and 90 mm, respectively. The sound absorption coefficients of these five structures were obtained through theoretical analysis, and the results are presented in **Figure 2**. It can be observed that the medium and high frequency incident waves are easily absorbed by the original SBH. However, absorption of low-frequency sound waves is quite poor. As the opening diameter of the SBH decreases, the first natural frequency of the SBH gradually decreases, dropping from 598 Hz at full opening to 254 Hz when the opening diameter is 30 mm. The ability to absorb low-frequency sound

waves has been significantly improved. Compared with the original SBH structure, the modified SBHs proposed in this paper have better low-frequency absorption performance.

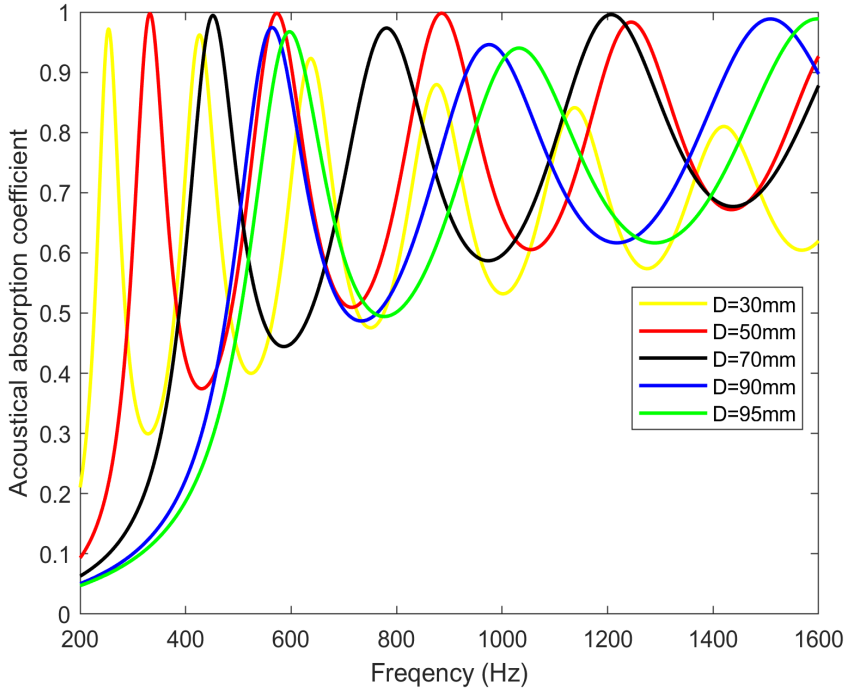

Figure 2. Absorption coefficients for different SBHs.

Next, we investigate how variations in the inlet opening diameter optimize low-frequency sound absorption performance. For the modified SBH model with a fixed geometric length, models with different opening diameters correspond to gradient rings of different proportions; extending these rings yields the original SBH, as illustrated in **Figure 3a** and the resulting length is referred to as the equivalent length L_{eq}:

$$L_{\text{eq}} = \frac{R_{SBH}}{R_{\text{inlet}}} L_{SBH} \tag{8}$$

where R_{SBH} is the maximum inner diameter of the SBH.

In order to obtain the SBH with an equivalent length, we set R_{inlet} = 25 mm. We then used theoretical calculations to compare the performance of sound absorption; the results are shown in **Figure 3b**. It is evident that the modified SBH with D = 50 mm has the same low-frequency sound absorption performance as the SBH at the same length, but its high-frequency performance is partially reduced because of the truncation of the front rings. This shows that the goal of improving low-frequency sound absorption performance without adding structural complexity can be accomplished by making the modified SBH equivalent to an original SBH of different lengths by changing the inlet aperture diameter.

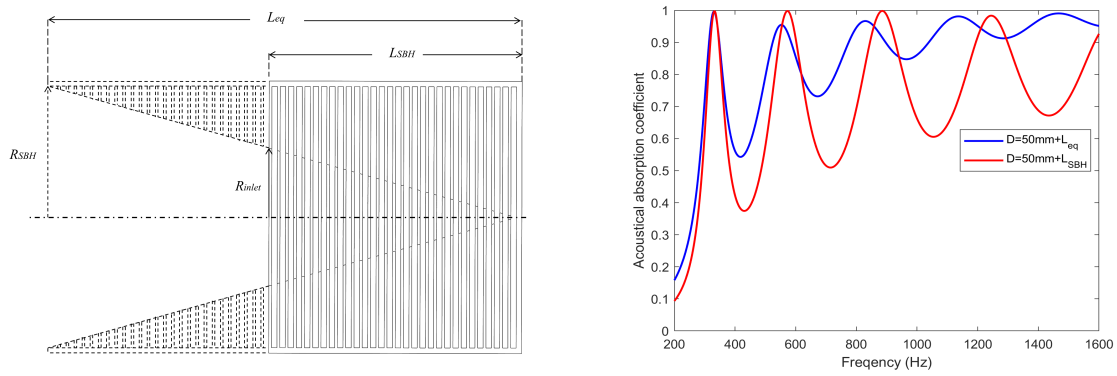

(a) **(b)**

Figure 3. **(a)** Schematic illustration of the equivalent-length SBH and modified SBH model; **(b)** Absorption coefficients for both the modified and equivalent-length SBH at D = 50 mm.

To examine the modified SBH structure's sound absorption mechanism in more detail, the reflection coefficient of the structure $R = \frac{\left(Z_{in} - \frac{Z_0}{S_0}\right)}{\left(Z_{in} + \frac{Z_0}{S_0}\right)}$ is analyzed in the complex frequency plane using complex frequency $f_c = f_r + j f_i$, where f_r corresponds to the natural frequency of the structure, and the imaginary part of the frequency f_i is introduced to reflect the energy attenuation rate. **Figure 4** shows the calculation results of $20\ \log_{10}(|R|)$ for the five structures proposed in this paper in the complex frequency plane. The reflection coefficient clearly shows several pairs of zeros and poles in the complex frequency plane. By comparing **Figure 4**, it can be seen that the modified SBH structure shows more zero-pole pairs than the original SBH structure within the same frequency range. Moreover, as the inlet opening diameter decreases, the resonance modes exhibited by the modified SBH structure tend to shift toward lower frequencies, and the attenuation of low-frequency sound waves gradually increases.

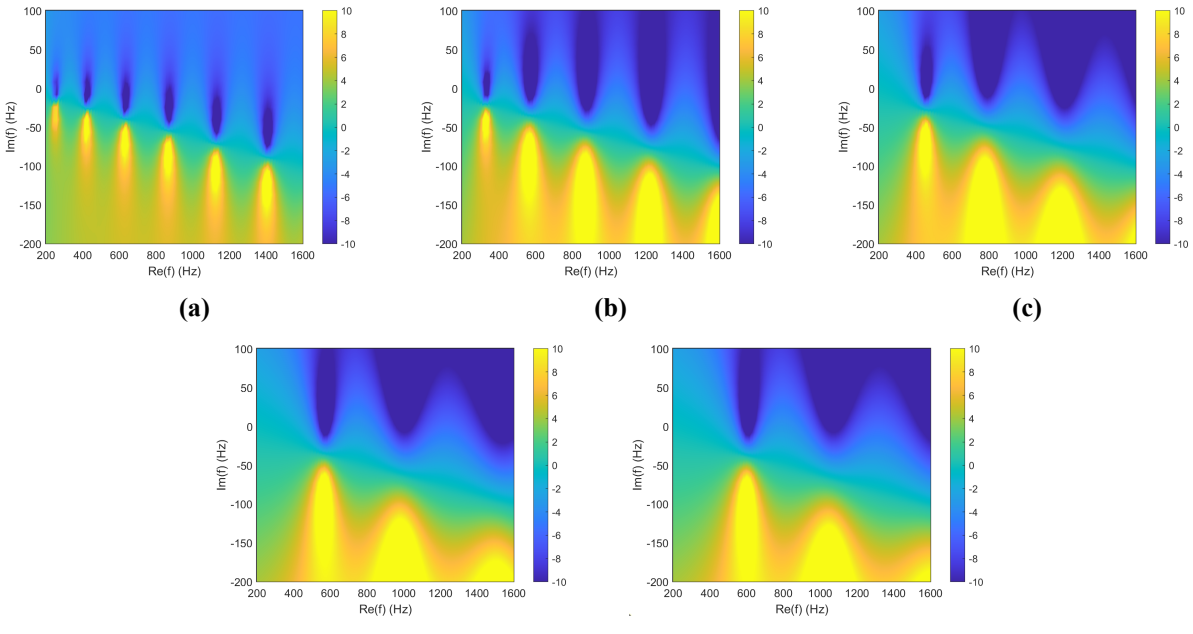

(a) **(b)** **(c)**

(d) **(e)**

Figure 4. Contour of $20\ \log_{10}(|R|)$ in the complex frequency plane for **(a)** D = 30 mm; **(b)** D = 50 mm; **(c)** D = 70 mm; **(d)** D = 90 mm and **(e)** D = 95 mm.

3.2. Sound pressure and particle velocity distribution in the modified SBH structure

In the preceding study, we used TMM to calculate the suggested modified SBH structure's sound absorption coefficient. We now proceed to perform numerical analysis of this structure through the finite element method (FEM).

Here, we utilize the COMSOL Multiphysics, a commercial software, to conduct finite element simulations on the proposed sound absorption structure. Under the plane wave assumption, we establish a two-dimensional (2D) finite element model and the geometric model is constructed based on the air domain. Considering that air flows through the model in practical situations, friction with the inner surfaces of the model is inevitable, resulting in thermoviscous losses, we perform a multi-physics coupling simulation by combining pressure acoustics and thermoviscous acoustics.

In this model, the thermoviscous acoustics is applied to the internal air domain of the structure, while the pressure acoustics is used for the background acoustic field. The sound source is implemented via a port boundary with an incident plane wave amplitude of 1 Pa. Leveraging the symmetry of the SBH structure, only half of the SBH model is simulated here to reduce computational cost. The mesh discretization of the air domain, as shown in **Figure 5**, adheres to the general acoustic meshing rule where the maximum element size is less than λ/6 (λ being the wavelength). This approach ensures both numerical accuracy and computational efficiency.

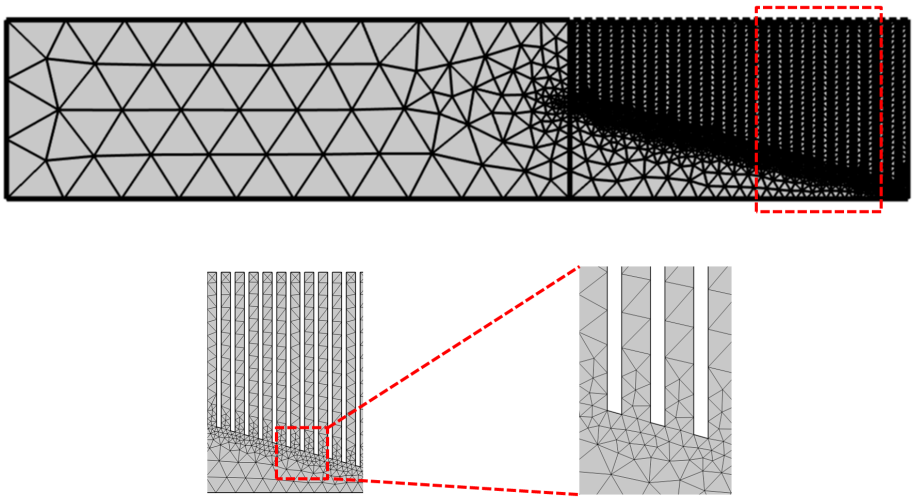

Figure 5. Finite Element Method (FEM) mesh generation.

Figure 6 illustrates the sound pressure distributions of the modified SBH structures with inlet opening diameters of D = 30 mm, 50 mm, 70 mm and 90 mm, as well as the original SBH structure with a fully open inlet end of D = 95 mm, at frequencies of 256 Hz, 332 Hz, 450 Hz, 558 Hz, and 596 Hz. It is evident that the incident sound waves are nearly entirely reflected at low frequencies, and the original SBH structure has a uniform sound pressure distribution. As the inlet opening diameter of the modified SBH decreases, high-pressure sound zones gradually appear in the middle and rear parts of the structure, where the incident sound energy is accumulated and dissipated, thereby achieving the goal of improving low-frequency

sound absorption performance. Because sound waves have a short wavelength, all SBH structures perform reasonably well at the mid-frequency of 596 Hz.

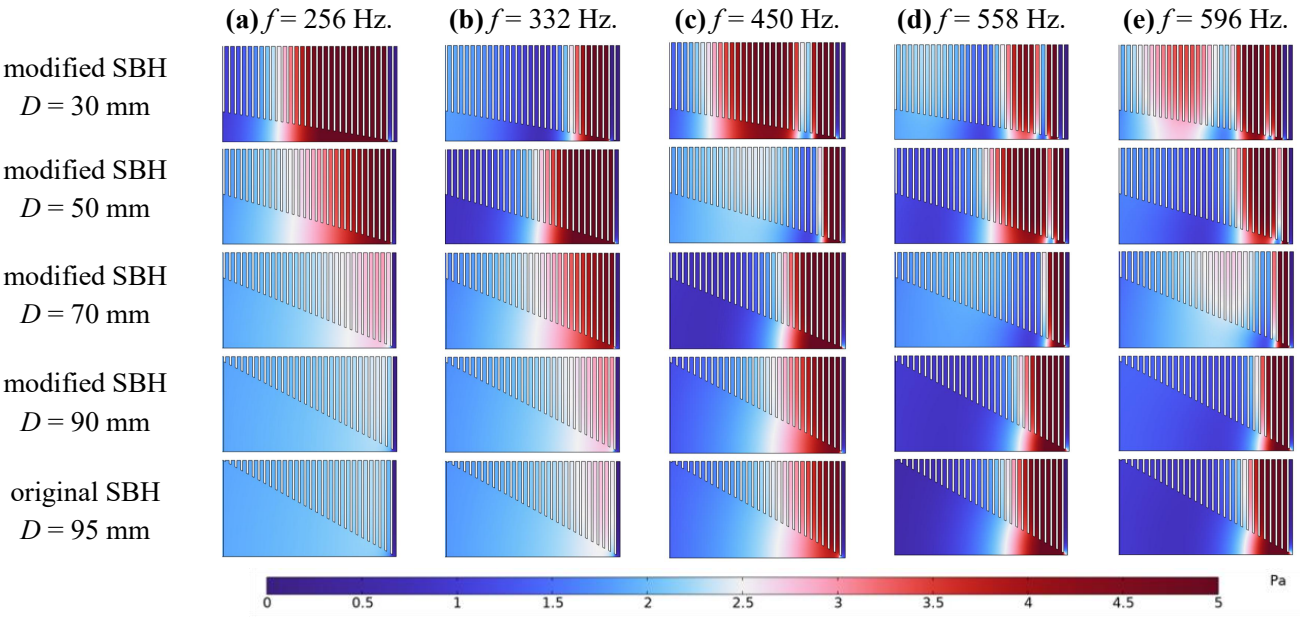

Figure 6. The sound pressure distribution of the modified SBH and original SBH at **(a)** f = 256 Hz; **(b)** f = 332 Hz; **(c)** f = 450 Hz; **(d)** f = 558 Hz and **(e)** f = 596 Hz.

Similarly, in order to learn more about the modified SB's low-frequency sound absorption mechanism, **Figure 7** presents the particle velocity diagrams of these five models at different peak frequencies, with the vector directions indicated by arrows. **Figure 7a** shows that at a frequency of 256 Hz, where the low-frequency sound waves have longer wavelengths, the modified SBH structure with a smaller inlet opening diameter exhibits a higher internal sound velocity. This is attributed to the significant changes in the internal structure, which lead to drastic variations in impedance. Low-frequency sound waves are strongly reflected within the structure as a result of these modifications, forcing the energy to be trapped inside and eventually dissipated gradually. Therefore, for low-frequency sound waves, the modified SBH structure with a smaller diameter exhibits superior sound absorption performance. As can be seen from **Figure 7c–e**, the SBH structure inherently possesses an adaptive advantage for non-low-frequency sound waves, as the energy is easily dissipated within the structure, resulting in generally high sound absorption coefficients.

In conclusion, the synergistic interaction between structural parameters and acoustic wave properties is the source of the modified SBH structure's sound absorption mechanism. The first resonance frequency is positively correlated with the opening diameter of the incident end. Reducing the inlet opening diameter lowers the natural frequency of the structure, making it more suitable for low-frequency sound waves. The drastic changes in impedance of the small-diameter structures induce strong reflections, causing sound energy to accumulate in the middle and rear parts to form high-pressure zones. The increased sound particle velocity prolongs the energy retention time, which is then dissipated through viscous losses and structural damping. The complex frequency diagram shows that it has more zero-pole pairs, and as the diameter decreases, the resonance modes shift toward lower frequencies, enhancing

the attenuation of low-frequency sound waves. At medium and high frequencies, where the sound wave wavelengths are short, all SBH structures easily trap energy due to their inherent characteristics, exhibiting a universal sound absorption advantage. In summary, the modified SBH optimizes resonance and energy dissipation in the low-frequency range by adjusting its structural dimensions, thereby enhancing sound absorption performance in that range.

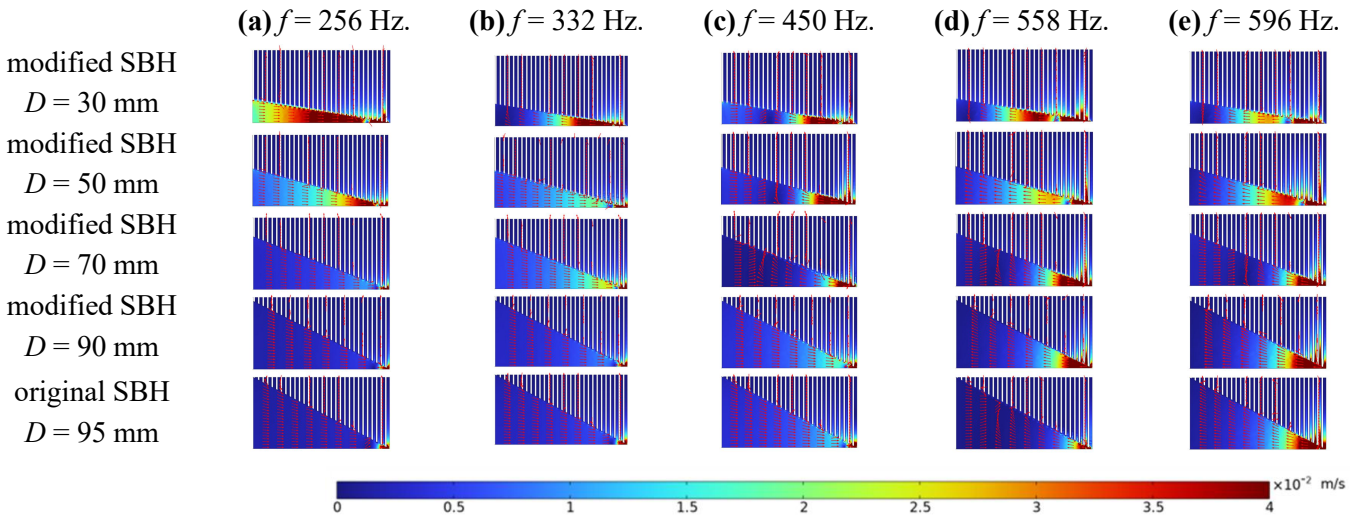

Figure 7. The particle velocity distribution of the modified SBH and original SBH at **(a)** f = 256 Hz; **(b)** f = 332 Hz; **(c)** f = 450 Hz; **(d)** f = 558 Hz and **(e)** f = 596 Hz.

4. Experimental setup and results

In accordance with the international standard ISO 10534-2, experimental measurements of the proposed modified SBH structures were conducted using the transfer function method. The main experimental equipment includes: AWA8551(T) type standard impedance tube, AWA6290B type multi-channel signal analyzer, and AWA5871 type power amplifier. In addition, a sound calibrator, microphones, signal analysis software and signal generation software were also configured. Among these, the sound calibrator is first used to calibrate the sensitivity of the microphones and eliminate system errors. **Figure 8** depicts the experimental setup and the SBH samples, respectively.

The measured sound absorption coefficient results for the five configurations are presented in **Figure 9**. In terms of the general trend, the experimental and theoretical results are in good agreement. The results indicate that the SBH's internal gradient structure gives it a natural advantage in capturing high-frequency sound waves. Clearly, reducing the opening diameter of the SBH causes the first resonance frequency to turn toward the lower frequency. For example, when the opening is fully open (D = 95 mm), the first resonance frequency is 615 Hz. When the opening diameter decreases to 90 mm, 70 mm, 50 mm and 30 mm, respectively, the corresponding first resonant frequency decreases to 610 Hz, 454 Hz, 293 Hz and 225 Hz, respectively. Compared with the original SBH (D = 95 mm), the effective absorption frequency is reduced by 63% when D = 30 mm. In other words, SBH structures with smaller opening

areas are better suited for low-frequency sound waves; this effectively enhances the sound absorption performance of the original SBH structure in the low-frequency range, thereby providing a practical method for improving the sound absorption performance of SBH structures in this frequency band.

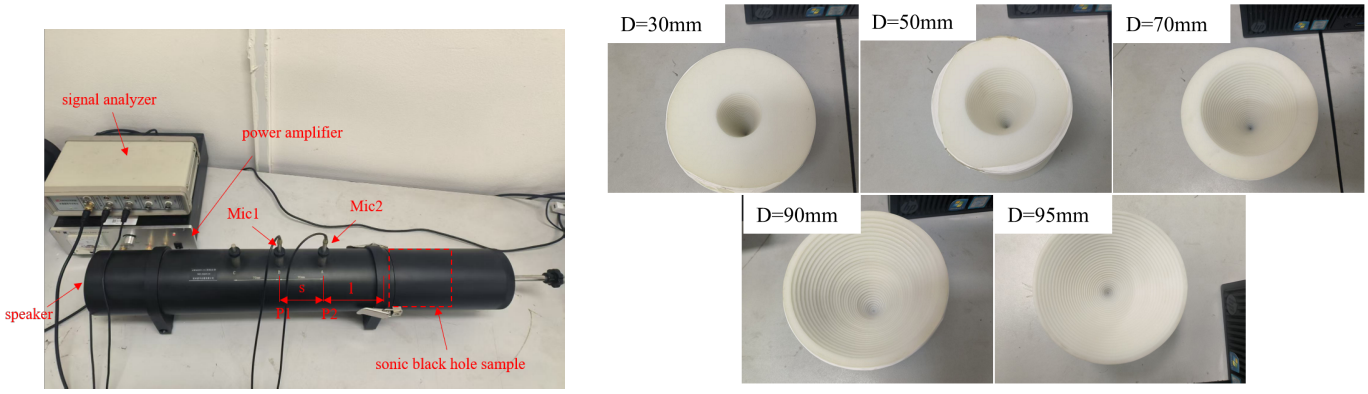

Figure 8. **(a)** Experimental setup and **(b)** SBH sample.

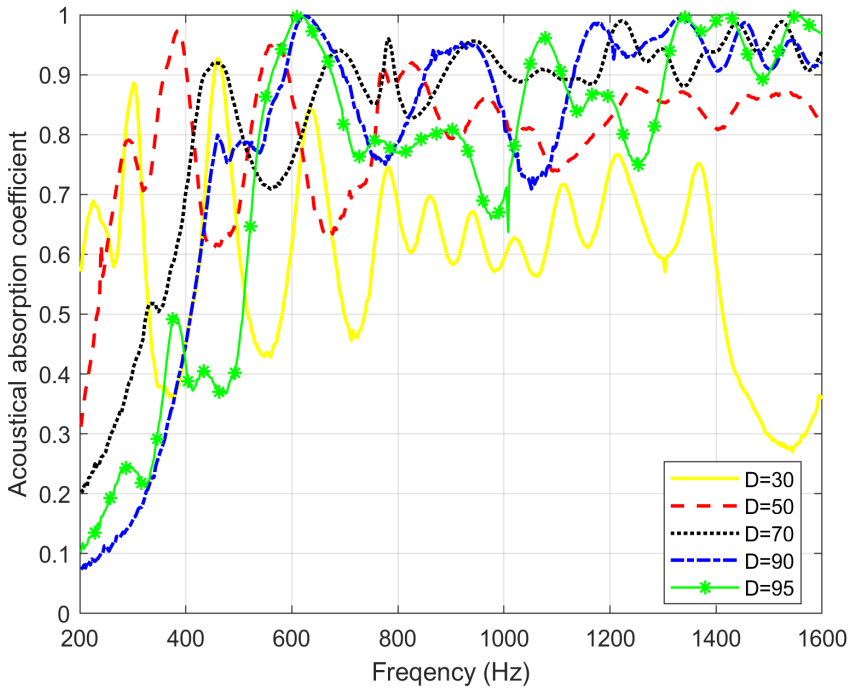

Figure 9. The measured sound absorption coefficients for different SBH samples.

However, it is worth noting that the results of the experiment and the results of the theoretical analysis cannot be completely matched in terms of sound absorption values. There are two main reasons why the experimental results exhibit more resonance peaks than the theoretical results: (1) Due to manufacturing defects in the SBH during the 3D printing process, the spacing and radius of the internal rigid rings deviated slightly from the theoretical values, resulting in new local resonance modes. And, the reduced opening area at the inlet increases the difficulty of printing internal structures, these manufacturing tolerances are magnified. (2) The boundary friction between the SBH sample and the impedance tube test section generates additional acoustic resonance,

which is not considered in the theoretical and simulation models. The above factors lead to discrepancies between the two results. The experimental results show additional resonance peaks compared to the theoretical results. The resulting errors will be further optimized in future research.

Furthermore, it can also be observed from **Figure 9** that although reducing the diameter of the incident end can improve the SBH structure's low-frequency sound absorption effect, when D = 30 mm, the high-frequency sound absorption of the modified SBH structure decreases significantly. This is also consistent with the theoretical analysis results. In order to enhance low-frequency sound absorption performance without increasing the complexity or geometric length of the SBH, we reduced the opening area at the incident end to extend the equivalent length of the proposed modified SBH. This enhances the coupling effect between the structure and low-frequency sound waves, shifts the resonance frequency downward, and ultimately optimizes sound absorption performance at low frequencies. However, when D = 30 mm, the absence of the front rings in the SBH results in a slight decrease in sound absorption performance in the high-frequency range.

5. Conclusion

This paper presents a modified SBH designed to enhance sound absorption performance in the low-frequency range. The acoustic characteristics of this modified SBH were analyzed using both theoretical and experimental methods. A theoretical model of the modified SBH is established based on the TMM. The concept of equivalent length was introduced, noting that reducing the inlet diameter is equivalent to increasing the equivalent acoustic length, which can enhance low-frequency coupling but results in some loss of high-frequency performance. In addition, a detailed study was conducted on the effect of opening diameters on sound absorption characteristics, and the results have been experimentally verified. The results indicate that a reduction in opening diameter leads to a decrease in the resonance frequency. When the opening diameter was reduced from its maximum value (95 mm) to 30 mm, the resonance frequency of the SBH decreased from 615 Hz to 225 Hz.

Author contributions: Conceptualization and methodology, QM; software and validation, ZC and LP; visualization and writing—original draft preparation, ZC; supervision and writing—review and editing, QM. All authors have read and agreed to the published version of the manuscript.

Funding: This work was funded by the National Natural Science Foundation of China (Grant No. 12364058); The Jiangxi Provincial Natural Science Foundation Project of China (Grant No. 20252BAC250009); The Innovation Special Fund project of Nanchang Hangkong University (Grant No. YC2025-S178).

Institutional review board statement: Not applicable.

Informed consent statement: Not applicable.

Data availability statement: All data that support the findings of this study are

included within the article.

Conflict of interest: The authors declare no conflict of interest.

AI use statement: The authors declare that no artificial intelligence (AI) tools were used in the preparation of this manuscript.

References

1. Sagartzazu X, Hervella-Nieto L, Pagalday JM. Review in Sound Absorbing Materials. Archives of Computational Methods in Engineering. 2008; 15(3): 311–342. doi: 10.1007/s11831-008-9022-1
2. Cummer SA, Christensen J, Alù A. Controlling sound with acoustic metamaterials. Nature Reviews Materials. 2016; 1(3): 16001. doi: 10.1038/natrevmats.2016.1
3. Yang M, Sheng P. Sound Absorption Structures: From Porous Media to Acoustic Metamaterials. Annual Review of Materials Research. 2017; 47(1): 83–114. doi: 10.1146/annurev-matsci-070616-124032
4. Mironov MA, Pislyakov VV. One-dimensional acoustic waves in retarding structures with propagation velocity tending to zero. Acoustical Physics. 2002; 48(3): 347–352. doi: 10.1134/1.1478121
5. Su L, Chen J, He X, et al. The acoustic streaming effects of sonic black hole. Modern Physics Letters B. 2022; 36(20): 2250079. doi: 10.1142/S0217984922500798
6. Peng L, Mao Q, Wang H, et al. Enhanced sound absorption with the combined sonic black holes. Applied Acoustics. 2024; 219: 109932. doi: 10.1016/j.apacoust.2024.109932
7. Bednarik M, Cervenka M. A sonic black hole of a rectangular cross-section. Applied Mathematical Modelling. 2024; 125: 529–543. doi: 10.1016/j.apm.2023.09.005
8. Yu Y-H, Huang W, Xie L-X, et al. Broadband sound absorption and slow wave in truncated sonic black hole. Applied Acoustics. 2025; 235: 110677. doi: 10.1016/j.apacoust.2025.110677
9. Deng J, Li J, Gao N, et al. A plug-in sonic black hole for duct terminations. Applied Acoustics. 2026; 243: 111119. doi: 10.1016/j.apacoust.2025.111119
10. Li S, Zhao J, Liu Z, et al. Coupling effects and optimized design of hexagonal sonic black holes with multiple exponents distribution. Journal of Sound and Vibration. 2026; 624: 119522. doi: 10.1016/j.jsv.2025.119522
11. Zhang KD, Yang JS, Chen SJ, et al. A synergistic composite sonic black hole metastructure for sub-wavelength broadband sound absorption. Wave Motion. 2026; 143: 103718. doi: 10.1016/j.wavemoti.2026.103718
12. Peng L, Mao Q. Helmholtz Resonator with Sonic Black Hole Neck. The International Journal of Acoustics and Vibration. 2023; 28(4): 460–468. doi: 10.20855/ijav.2023.28.42006
13. Liang X, Liang H, Chu J, et al. A modified sonic black hole structure for improving and broadening sound absorption. Applied Acoustics. 2023; 210: 109440. doi: 10.1016/j.apacoust.2023.109440
14. Liang X, Chu J, Ouyang X, et al. Sound absorption mechanism of sonic black hole with labyrinthine units and micro perforated panel. International Journal of Modern Physics B. 2024; 38(23): 2450305. doi: 10.1142/S0217979224503053
15. Jin J, Zhu Z, Cao Y, et al. A novel labyrinth-type structure enhancing sound insulation properties with acoustic black hole and Herschel-Quincke tube principles. Applied Acoustics. 2025; 240: 110972. doi: 10.1016/j.apacoust.2025.110972
16. Meng D, Liang X, Liang H, et al. Broadband sound absorption using acoustic black holes with micro-perforated panels. Modern Physics Letters B. 2024; 38(26): 2450243. doi: 10.1142/S0217984924502439
17. Chen Y, Yu K, Fu Q, et al. Broadband and low-frequency sound absorber by a rectangular sonic black hole combined with labyrinth metasurface. Mechanical Systems and Signal Processing. 2025; 239: 113301. doi: 10.1016/j.ymssp.2025.113301
18. Petrover K, Baz A. Acoustic Black Hole With Functionally Graded Perforated Rings: Modeling and Experimental Performance. Journal of Vibration and Acoustics. 2025; 147(5): 050501. doi: 10.1115/1.4068869
19. Petrover K, Baz A. Acoustic black hole with functionally graded perforated rings and sound absorbing layers: Theory and experiments. Journal of Low Frequency Noise, Vibration and Active Control. 2025; 44(4): 2261–2279. doi: 10.1177/14613484251340116
20. Li S, Xia J, Yu X, et al. A sonic black hole structure with perforated boundary for slow wave generation. Journal of

Sound and Vibration. 2023; 559: 117781. doi: 10.1016/j.jsv.2023.117781
21. Ou Y, Zhao Y. Design, analysis, and experimental validation of a sonic black hole structure for near-perfect broadband sound absorption. Applied Acoustics. 2024; 225: 110196. doi: 10.1016/j.apacoust.2024.110196
22. Wu WQ, Zhang YB, Zhao LX, et al. Sonic black hole coupled with membrane-type acoustic metamaterial for broadband and low-frequency sound absorption. Mechanical Systems and Signal Processing. 2026; 246: 113932. doi: 10.1016/j.ymssp.2026.113932
23. Zhang X, Wang L, Cheng L, et al. Acoustic muffling of the Sonic Black Holes. Applied Acoustics. 2025; 240: 110949. doi: 10.1016/j.apacoust.2025.110949
24. Maury C, Bravo T, Amielh M, et al. Acoustic Pressure Amplification through In-Duct Sonic Black Holes. Applied Sciences. 2024; 14(11): 4699. doi: 10.3390/app14114699
25. Zhou Z, Hu N, Yang Y, et al. Sonic black hole based metamaterial structure for contactless rotating machinery state sensing enhancement. Measurement. 2026; 259: 119613. doi: 10.1016/j.measurement.2025.119613
26. Peng L, Mao Q, Chen Z, et al. Piezoelectric sonic black hole for broadband energy harvesting. Sensors and Actuators A: Physical. 2026; 399: 117487. doi: 10.1016/j.sna.2026.117487
27. Mao Q, Peng L. Broadband and high-efficiency acoustic energy harvesting with loudspeaker enhanced by sonic black hole. Sensors and Actuators A: Physical. 2024; 379: 115888. doi: 10.1016/j.sna.2024.115888
28. Umnova O, Brooke D, Leclaire P, et al. Multiple resonances in lossy acoustic black holes - theory and experiment. Journal of Sound and Vibration. 2023; 543: 117377. doi: 10.1016/j.jsv.2022.117377
29. Guasch O, Arnela M, Sánchez-Martín P. Transfer matrices to characterize linear and quadratic acoustic black holes in duct terminations. Journal of Sound and Vibration. 2017; 395: 65–79. doi: 10.1016/j.jsv.2017.02.007
30. Mi Y, Cheng L, Zhai W, et al. Broadband low-frequency sound attenuation in duct with embedded periodic sonic black holes. Journal of Sound and Vibration. 2022; 536: 117138. doi: 10.1016/j.jsv.2022.117138
31. Chen Y, Yu K, Fu Q, et al. Modification of the transfer matrix method for the sonic black hole and broadening effective absorption band. Mechanical Systems and Signal Processing. 2024; 220: 111660. doi: 10.1016/j.ymssp.2024.111660